

Article

Small Hall Effect Thruster with 3D Printed Discharge Channel: Design and Thrust Measurements

Ethan P. Hopping¹, Wensheng Huang² and Kunning G. Xu^{3,*} 

¹ Aerospace Engineering Department, Georgia Institute of Technology, Atlanta, GA 30332, USA; ethan.hopping@gatech.edu

² NASA Glenn Research Center, Cleveland, OH 44135, USA; wensheng.huang@nasa.gov

³ Mechanical and Aerospace Engineering Department, University of Alabama in Huntsville, Huntsville, AL 35899, USA

* Correspondence: gabe.xu@uah.edu

Abstract: This paper presents the design and performance of the UAH-78AM, a low-power small Hall effect thruster. The goal of this work is to assess the feasibility of using low-cost 3D printing to create functioning Hall thrusters, and study how 3D printing can expand the design space. The thruster features a 3D printed discharge channel with embedded propellant distributor. Multiple materials were tested including ABS, ULTEM, and glazed ceramic. Thrust measurements were obtained at the NASA Glenn Research Center. Measured thrust ranged from 17.2–30.4 mN over a discharge power of 280 W to 520 W with an anode I_{sp} range of 870–1450 s. The thruster has a similar performance range to conventional thrusters at the same power levels. However, the polymer ABS and ULTEM materials have low temperature limits which made sustained operation difficult.

Keywords: hall thruster; electric propulsion; additive manufacturing



Citation: Hopping, E.P.; Huang, W.; Xu, K.G. Small Hall Effect Thruster with 3D Printed Discharge Channel: Design and Thrust Measurements. *Aerospace* **2021**, *8*, 227. <https://doi.org/10.3390/aerospace8080227>

Academic Editor: Igor Levchenko

Received: 22 July 2021

Accepted: 12 August 2021

Published: 15 August 2021

Publisher's Note: MDPI stays neutral with regard to jurisdictional claims in published maps and institutional affiliations.



Copyright: © 2021 by the authors. Licensee MDPI, Basel, Switzerland. This article is an open access article distributed under the terms and conditions of the Creative Commons Attribution (CC BY) license (<https://creativecommons.org/licenses/by/4.0/>).

1. Introduction

Hall effect thrusters (HET) are a type of electric propulsion device currently used for satellite propulsion and station-keeping. Small HETs have gained interest in the last 20 years with the rise of small satellites. There are now multiple companies such as Apollo Fusion, Orbion, Exotrail, Busek, and Sitael SpA, that develop hall HETs. Notably, SpaceX has successfully launched over 1000 small HETs on their Starlink constellation satellites. One of the advantages of small satellites is their significantly lower cost of design and production. However, HETs are still traditionally subtractive manufactured using the same materials as 30 years ago. One source of manufacturing cost and time for HETs are the anode and discharge channel assemblies. In most Hall thrusters, the propellant distributor is integrated into the anode assembly. This requires multi-part fabrication and welding to integrate the baffle assemblies, orifices, and other distributor assemblies into the anode. The discharge channels of most SPT type HETs are made of boron nitride, a hot-pressed ceramic that must be subtractively machined from a single block. Monolithic boron nitride dimensions are limited by the hot-pressing process, and this poses challenges for the design of large thrusters [1,2]. In addition, the cost of the boron nitride components increases substantially with thruster size.

In other aerospace industries, additive manufacturing (AM), or colloquially 3D printing, is being used to dramatically reduce the cost of components [3]. Propulsion systems are well suited to the AM processes due to their complex geometry and low-volume production. In this research, we seek to investigate the use of 3D printing to reduce the cost of HET fabrication, with a focus on using low-cost and fast turnaround methods. If AM can reduce the part count and simplify the design and fabrication of the thruster, not only will it bring down the cost of the device, but also enable agile development and test programs of new thruster designs.

2. Materials and Methods

2.1. Thruster Design

The UAH-78AM is an annular HET designed to fit in CubeSat dimension, $10 \times 10 \times 10$ cm. The thruster is a loose scaling of the channel of the P5 HET [4]. The magnetic field topology is copied from the P5. It has a design discharge power of 300–500 W. Images of the thruster are provided in Figure 1, and an isometric view of the design tested at the NASA Glenn Research Center (GRC) is provided in Figure 2. The “AM” designation stands for additively manufactured, and the “78” is the diameter of the outer channel in millimeters.



Figure 1. Testing of the UAH-78AM at GRC.

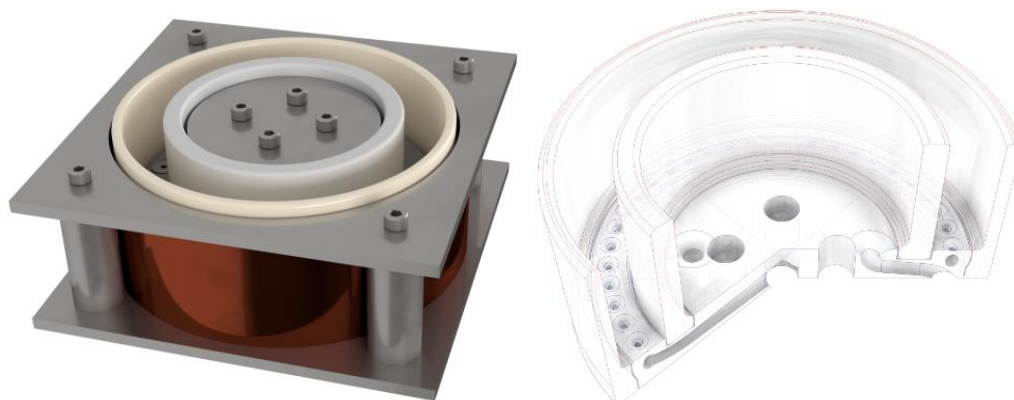


Figure 2. 3D rendering of UAH-78AM configuration as tested at GRC and a cross-section of the discharge channel with embedded propellant distributor and inner and outer channel walls.

2.1.1. 3D Printed Discharge Channel and Materials

The discharge channel with embedded propellant distributor was the focus of the 3D printing. This was primarily due to the lack of accessible printing of ferromagnetic materials such as iron or low carbon steel. In SPT-type Hall thrusters, the discharge channel is made of ceramic materials with high secondary electron emission (SEE). The high SEE reduces the average electron temperature in the plasma, which increases ionization efficiency [5–7]. This means the material selection is limited to dielectrics with high SEE. Polymers provide SEE profiles similar to ceramics, but they also present design challenges due to low melting temperatures.

There is little information in the literature on the SEE characteristics of polymers in the incident electron temperature range of Hall thrusters. This is likely because most SEE data is intended for scanning electron microscope applications, where minimum primary electron energy is on the order of 100 eV or more. An estimate for the SEE characteristics of polymers in the 0–100 eV range was thus made by extrapolating the attenuation model by Cazaux [8]. The SEE results of the model for Nylon-12 and PTFE are presented in Figure 3 along with boron nitride and Borosil ceramics from by Goebel and Katz [9].

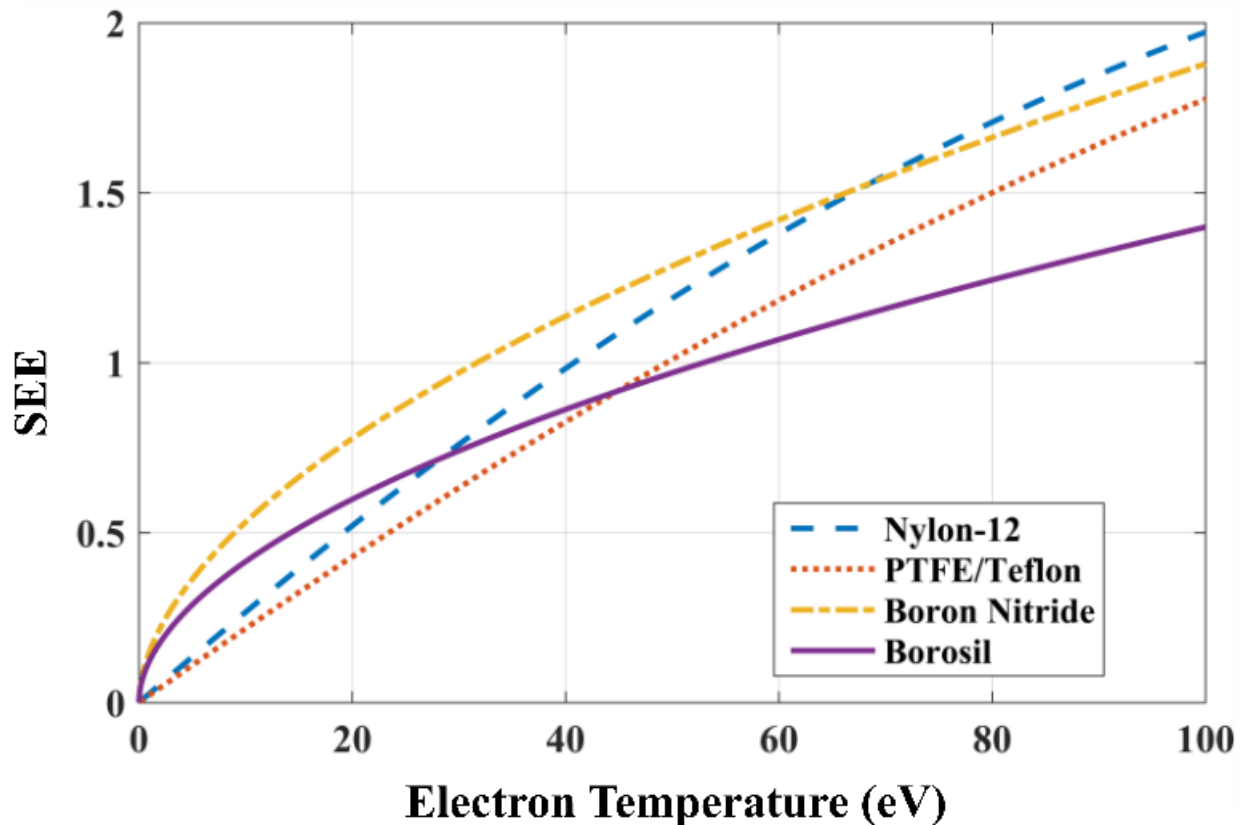


Figure 3. Extrapolated secondary electron emission as a function of temperatures for selected polymers below 100 eV.

As the figure shows, the SEEs for both polymers are comparable to the ceramics from approximately 40–100 eV. At energies below 40 eV, the ceramics have higher SEE, but the difference is less than a factor of two. These results indicate that polymer SEE profiles are comparable to common HET ceramic material in the electron temperature range seen in thrusters. Data for ABS and ULTEM polymer were not available, thus could not be directly compared, but we expected their SEEs to be similar to Nylon and PTFE as they have similar chemical composition.

The discharge channel was printed in three parts: the rear of the channel with embedded propellant distributor, the inner channel wall, and the outer channel wall. The embedded propellant distributor allowed us to use a simple stainless-steel ring as the anode, thus separating propellant injection from the anode. All parts were initially printed with ABS plastic. However, testing revealed that the ABS's relatively low glass transition temperature of 105 °C limited the lifetime of the channel. The plasma heating caused charring and melting of the channel, especially at the exit plane where the magnetic field was strongest and thus has the highest temperature. Higher temperature 3D printable dielectric materials were considered. We settled on two materials: ULTEM with a glass transition temperature of ~200 °C, and a glazed ceramic.

Separate 3D printers were used for ULTEM and ABS parts. Part accuracy for the ULTEM printer is ± 0.130 mm or better. Accuracy for the ABS 3D printer is more difficult to

predict as this was not a commercial 3D printer. Therefore, factors such as belt backlash and part shrinkage are not taken into account when quoting accuracy. However, axis resolution is 0.01 mm, and since the 3D printing technology is functionally identical to the ULTEM 3D printer, part accuracy is likely comparable. The smallest features in our parts were the propellant distributor orifices, which had a diameter of 0.01 in (0.254 mm). Light sanding was used for part cleanup on polymer components in some areas to improve fit. The glazed ceramic, which is similar to pottery, was produced by an external vendor, i.Materialize. The ceramic was not actually 3D printed, but rather the mold was printed in plastic and then filled with a liquid ceramic mixture. After drying and hardening, the ceramic part undergoes a firing and glazing process to reach the finished state. The firing process naturally induces part shrinkage on the order of 3% of total part size and was accounted for in the design. In addition, minimum feature size was limited to approximately 2 mm by the vendor due to the need for the liquid ceramic to fill all spaces. Due to this large minimum feature size, the propellant distributor was not made in ceramic due to the more stringent tolerances required for the part. The propellant distributor (the rear of the discharge channel) also did not experience significant thermal heating during the initial tests, thus, was kept in ABS. The final thruster that was performance tested consisted of an ABS rear channel/propellant distributor, a glazed ceramic inner wall, and an ULTEM outer wall. This mixture allowed us to test the different materials, mainly the ceramic and ULTEM in a single set of tests.

2.1.2. Magnetic Field Design

The UAH-78AM's magnetic field is based on the design heritage from the P5. The front and back magnetic poles were changed to squares instead of circles to emulate the CubeSat geometry. The magnetic poles were made of low carbon 1018 steel and traditionally manufactured. Five 1018 steel rods were used to connect to front and back poles and complete the magnetic circuit. The magnetic field was simulated in both Finite Element Method Magnetics software, and Ansys to match the P5 fields. An inner electromagnet was wrapped around the center magnetic pole (not shown in Figure 2), and an outer electromagnet wrapped on the outside of discharge channel (the copper-colored part in Figure 2). To limit independent variables in testing, the inner and outer magnet currents were held fixed at 4.09 A for all tests to generate the desired channel magnetic field.

2.1.3. Cost and Turnaround Time

As one of the goals of this work is to reduce the cost and fabrication time of small HETs, Table 1 provides a cost breakdown for the UAH-78AM, in USD. All materials for the thruster in the United States can be procured for a total of \$300 or less. This cost assumes the availability of 3D printers and other machining equipment.

Table 1. UAH-78AM cost breakdown.

Material	Component	Cost	Notes
Carbon Steel	Magnetic Circuit	\$57	
Fasteners	Magnetic Circuit	\$30	
Magnet Wire	Magnetic Circuit	\$30	
Carbon Shim Stock	Magnetic Shields	\$15	
Stainless Steel	Anode	\$4	Fabricated from stainless steel washer
3D printed glazed ceramic	Inner Channel	\$21	Quote from manufacturer
ULTEM	Outer Channel	\$97	Quote from manufacturer
ABS	Inner Channel	\$2	By Volumetric Material Cost
Material Total		\$256	
Labor		\$560	35 \$/h for 16 h
Total		\$816	

Costs for the ULTEM outer channel and glazed ceramic inner channel are based on quotes directly from vendor. Consequently, these costs are significantly inflated as

compared to the true costs of materials and print time. It is increasingly common for academic institutions to have access to 3D printing services on campus or through business partnerships. These services frequently provide print services at material cost or less, so it is possible that the inner and outer channel components could be procured for much lower cost. ABS 3D printing is so broadly available through professional and hobbyist services that we provide the component price based on volumetric material cost.

The most significant labor costs are in fabrication of the magnetic circuit, which is cut using a conventional subtractive machining process. However, significant efforts were made in the design of the thruster to simplify machining operations as much as possible. Machining for the magnetic circuit is dominated by hole processes. While access to CNC machining simplifies manufacturing, all parts could be produced with relative ease using manual machines. We estimate that total labor time for a skilled machinist on magnetic circuit fabrication would be a day or two. However, labor remains the costliest portion of UAH-78AM procurement assuming an hourly rate of \$35 per hour. Experience from testing demonstrates that the thruster can be assembled from raw components in a week or less. In addition, the turnaround time for servicing between tests is on the order of a couple of days.

In comparison, a first order cost estimate is shown in Table 2 below if the UAH-78AM were to be fabricated using traditional manufacturing methods and with a traditional baffled anode that also functions as the propellant distributor.

Table 2. UAH-78AM cost breakdown.

Material	Component	Cost	Notes
Carbon Steel	Magnetic Circuit	\$57	
Fasteners	Magnetic Circuit	\$30	
Magnet Wire	Magnetic Circuit	\$30	
Carbon Shim Stock	Magnetic Shields	\$15	
Stainless Steel	Anode/Propellant Distributor	\$50	Thicker stock material to fabricate the baffled anode for propellant distribution
Boron Nitride Channel	Discharge Channel	\$1060	Estimated from prior purchases of boron nitride for larger thrusters
Material Total		\$1242	
Labor		\$3800	35 \$/h for 10 days, anode and magnetic circuit fabrication + \$1000 for orifice drilling
Total		\$5042	

2.2. Test Facility

Tests were conducted in Vacuum Facility 8 at NASA Glenn Research Center. The main chamber of VF-8 has a diameter of 1.5m and a length of 4.5 m. Pumping is provided by four oil-diffusion pumps with a speed of 1.2×10^5 L per second at 10^{-5} torr [10]. VF-8 features two bell-jars that can be independently isolated from the main chamber using gate valves. The thruster was mounted on an inverted-pendulum thrust stand attached to the vacuum flange of the primary bell jar. The design and operation of this type of thrust stand is well established in the literature, and further details on the design of similar stands at Glenn are provided in [11]. Anode and cathode propellant flow were provided by 100 sccm and 25 sccm mass flow controllers manufactured by Celerity, and all tests were run using Xenon.

A BaO cathode was used with a fixed flow rate of 0.5 mg/s for all tests. The cathode was oversized for the anode current required to sustain thruster discharge. Consequently, the discharge current was too low to allow for self-heating, thus requiring the cathode

heater to run at half-power during tests to ensure stable operation. Since cathode flow is not optimized, all specific impulses are presented in terms of the anode flow. It is likely that cathode flow could be reduced to 6–7% of anode flow while maintaining stable discharge.

3. Results and Discussion

The focus of the UAH-78AM testing was on powers and discharge voltages that could be sustained by small satellites. Furthermore, the low melting temperatures of the polymer materials limited operation at the higher power end due to higher channel wall heating [12]. The testing at GRC focused on identifying stable low-voltage operating points and flow rates and obtaining baseline performance parameters. It was found that 200 V and 1.82 mg/s anode flow produced a stable discharge at our chosen magnet settings. The thruster was run at points barely in the jet mode of hall thruster discharge, where efficiency is significantly improved from a diffuse mode but power requirements remain low [13]. Therefore, once the 200 V operating point was identified, discharge voltage was increased in 20 V increments from 180–260 V, and anode flow was increased in 0.18 mg/s increments between 1.64 and 2.18 mg/s.

Initial thrust measurements were taken in 5 s test intervals to limit thruster heating. After the 5 s data were collected for the desired test matrix, the operating time was increased to 15 s to get closer to steady-state behavior. Several thrust measurements were taken over longer durations on the order of 30 s to assess thrust stability in longer tests.

3.1. General Characteristics

A characteristic raw thrust curve is presented in Figure 4. This thrust measurement is from a 30-s test at a 200 V discharge and anode flow of 1.82 mg/s. Thrust stabilized at approximately 19 mN, but gradually climbed until the 30-s test conclusion. The increase in thrust is likely due to outgassing that increases as the polymer thruster components are heated. Similar behavior is seen in conventional HETs as water vapor and other volatile compounds outgas from the channel walls. The outgassing process is thought to modify the secondary electron behavior of the channel walls in boron nitride thrusters, resulting in artificially high discharge currents [14]. In an effort to reduce moisture content, we performed a 12-h low-temperature bake-out on the ABS components. The ULTEM outer channel was manufactured in a heated build chamber with temperatures approaching 200 °C, so it is expected that the moisture content in this component was low.

The outgassing processes may also be more complex in the UAH-78AM than evaporation of surface water or other contaminants from exposure to ambient air. What we refer to as outgassing may be a combination of sublimation and/or ablation processes that occur as the channel wall surface is heated beyond the glass transition temperature of the polymer. Chemical processes could also be playing a role, as the polymer gases could decompose into their constituent atoms as they diffuse into the channel. For lack of a better term, we will continue to refer to the process as outgassing; however, the physical process may be more complex than what is encountered in conventional Hall thrusters.

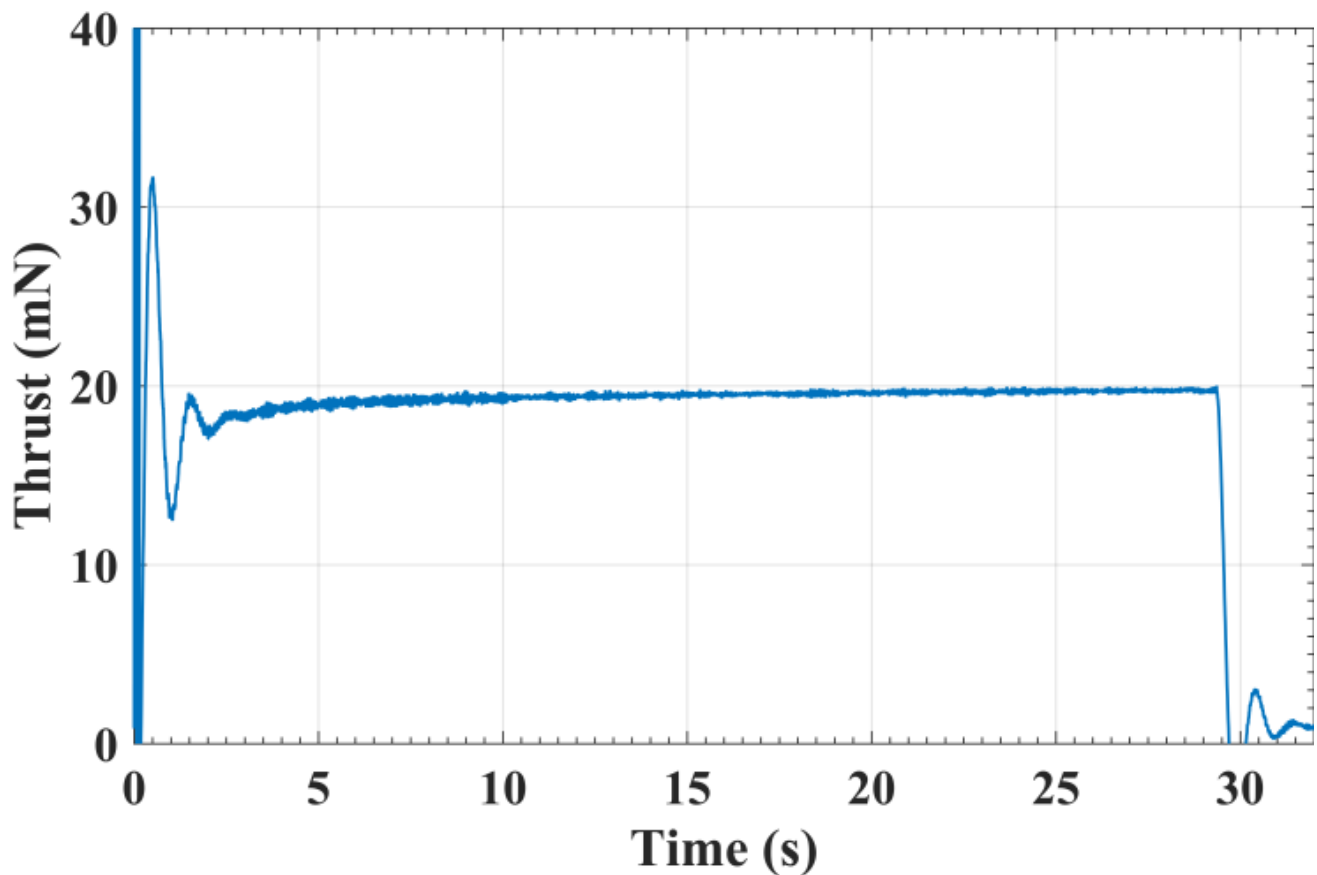


Figure 4. Thrust as a function of time at 200 V discharge voltage and anode flow of 1.82 mg/s.

The use of polymer materials in the thruster also presented unique challenges for measuring thrust. The heating of the polymer limited testing duration to 30 s. Beyond 30 s, a failure mode was observed where a hotspot attached to the outer ULTEM discharge channel wall and the thruster entered a current-limited mode of operation. Hotspot formation can be a problem in conventional Hall thrusters [1], but the cause is different as compared to the UAH-78AM. Hotspots are especially troubling with our thruster since the hotspot increased the polymer outgassing rate which encouraged continued spot formation and growth. If left unchecked, the hotspot permanently damages the discharge channels, and the polymer components must be replaced. An image of the spotting behavior is provided in Figure 5.

Without the ability to operate the thruster at steady-state, we choose to characterize performance by comparing thrust and specific impulse at fixed times after ignition. The ignition event is identified through a derivative approach. The derivative is taken of the thrust trace and time zero is identified as the location where the thrust rate of change exceeds 20 mN/s, as this behavior is only seen during thruster ignition. For the 5-s tests, thrust and specific impulse are measured 4 s after the ignition event. For the 15-s tests, measurements are taken 14 s after ignition. We expected thruster thermal conditions to be similar at fixed times after ignition, enabling comparison across different discharge voltages and flow rates. However, the heating rate and thermal condition of the channel likely varies between tests, resulting in some error in repeatability. We attempted to characterize this uncertainty through repeated tests, which are discussed later in the results. Calibration and measurement uncertainties associated with the equipment were calculated and reported according to the best practices identified in Refs. [15,16]. While thrust and I_{sp} uncertainty vary slightly with the calibration for each test run, the average thrust uncertainty at 95% confidence is ± 0.72 mN, and I_{sp} uncertainty is ± 40 s.

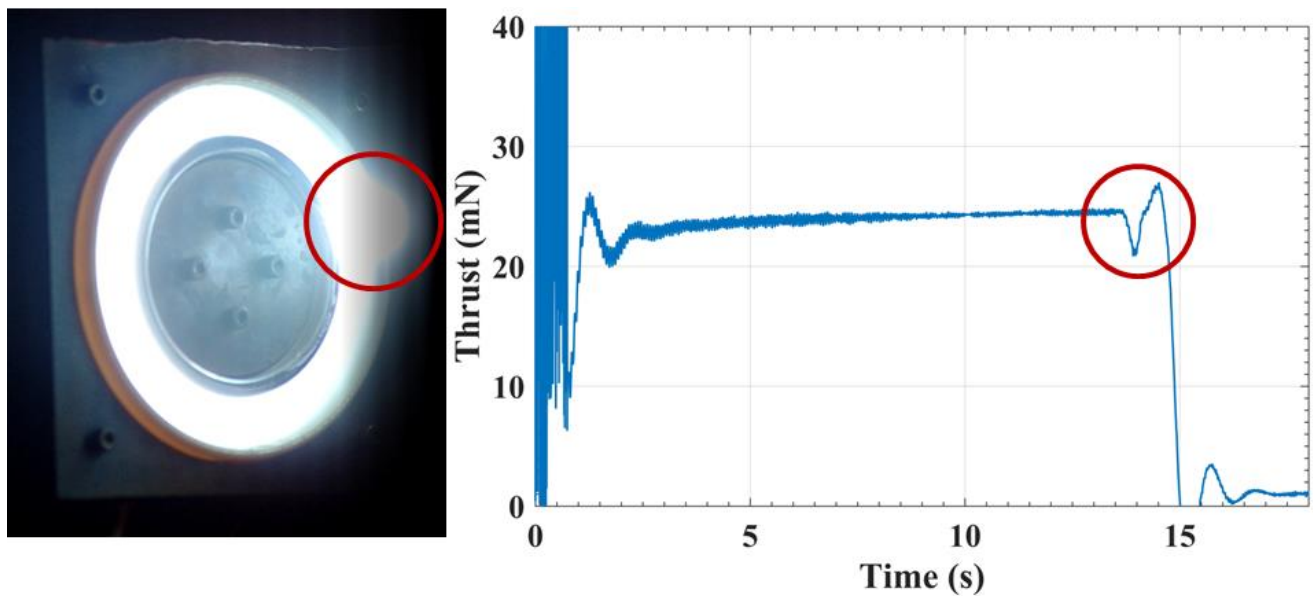


Figure 5. Image of hotspot formation and corresponding decrease in thrust.

3.2. Thrust

Figure 6 show the thrust as a function of anode discharge voltage and anode mass flow rate for the 5- and 15-s test runs. The general trends are as expected for HETs, with thrust increasing with both discharge voltage and flow rate. The thrust varied from 17.2–30.4 mN over the range of conditions tested.

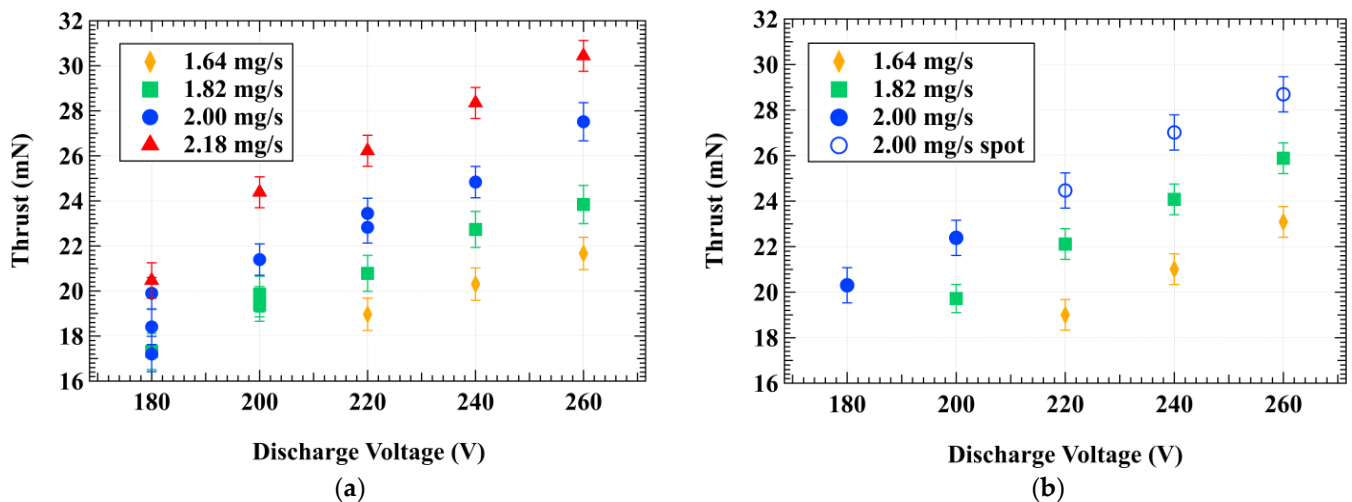


Figure 6. Thrust as a function of discharge voltage and anode mass flow rate from (a) the 5-s tests and (b) the 15-s tests.

Repeat tests were done for the 5-s data at 180, 200, and 220 V. At 180 V, the 2.00 mg/s repeat tests display a vertical spread of approximately 5 mN. The error bars in the figure do not account for the differences in thrust for the repeat tests. During testing, it was noticed that at 180 V the thruster took longer to start and for the discharge to settle. It is suspected that 180 V is the lower limit of the jet-mode discharge with the fixed magnet settings and the 2.00 mg/s anode flow rate, thus resulting in high variability. The repeat tests at 200 and 220 V fall within the equipment error, indicating that the short duration tests can produce consistent measurements at voltages above the limit. At 1.64 mg/s, the thruster could not be started at 180 or 200 V without adjusting magnet settings.

While collecting 15-s data at 220 V and 2.00 mg/s, a spot formed and attached to the outer channel wall. The thruster was turned off after spot formation and allowed to cool before starting again. A few more points were taken after the spot formation and are labeled with open circles in all plots. The damage to the ULTEM outer channel wall associated with spot formation could change the performance of the thruster by increasing anode leakage current. This would limit comparisons with preceding operating points. However, the data is included for completeness since the thruster was able to start and run without further spot formation after the channel had been allowed to cool. Due to the spot formation, 15-s tests were not done at 2.18 mg/s anode flow to prevent further heating of the channel wall as heating rate increases at higher discharge powers, which are associated with higher flow rates [12].

3.3. Anode Specific Impulse

The anode specific impulse (I_{SP}) is shown in Figure 7. The anode I_{SP} is calculated with $I_{SP} = T/(\dot{m}_a g_0)$, where \dot{m}_a is the anode mass flow rate and g_0 is Earth sea-level gravity. The I_{SP} ranges from 870–1450 s and increases with discharge voltage as expected. The data also suggest that I_{SP} increases with flow rate; however, the differences are within the measuring uncertainty.

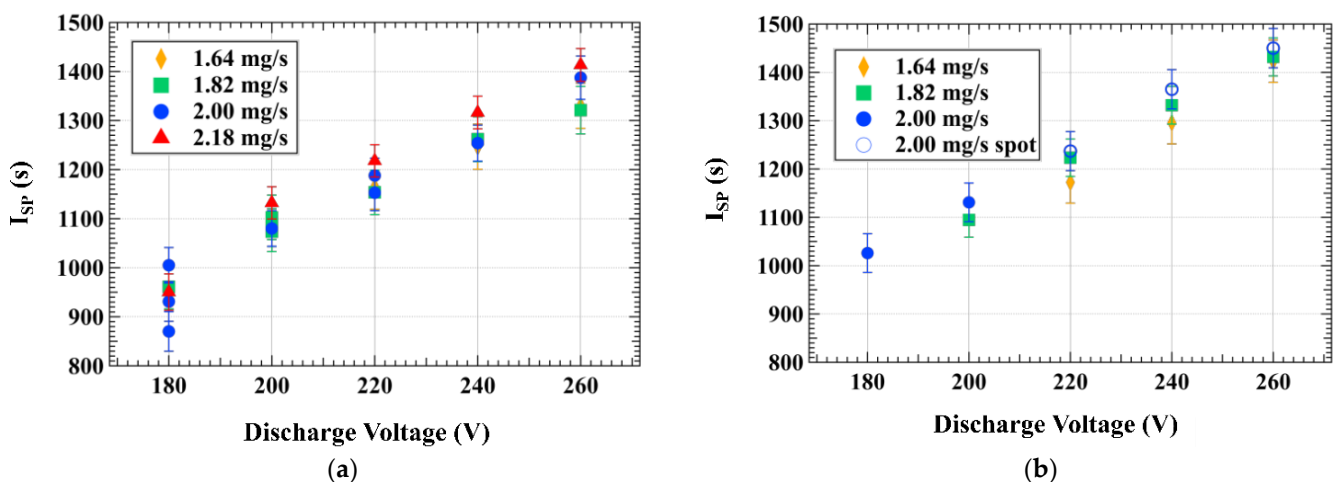


Figure 7. (a) Anode specific impulse as a function of discharge voltage and anode mass flow rate for 5-s tests; (b) Anode specific impulse for 15-s tests.

3.4. Anode Efficiency

The thrust anode efficiency, calculated from $\eta_a = T^2/(2\dot{m}_a P_d)$, where P_d is the discharge power is shown in Figure 8. The anode efficiency neglects additional power sources such as the cathode and magnets. Anode efficiency increased with discharge voltage and varied from 27.8–42.2%, with a few exceptions. In the 5-s tests at 1.82 mg/s, the efficiency was slightly lower at 260 V compared to 240 V. The same occurred in the 15-s tests at 2.00 mg/s. The latter measurement was taken after the spot formation, as indicated by the open circles. Thus, the loss in efficiency may be a product of increased anode leakage current due to the damage to the outer channel wall.

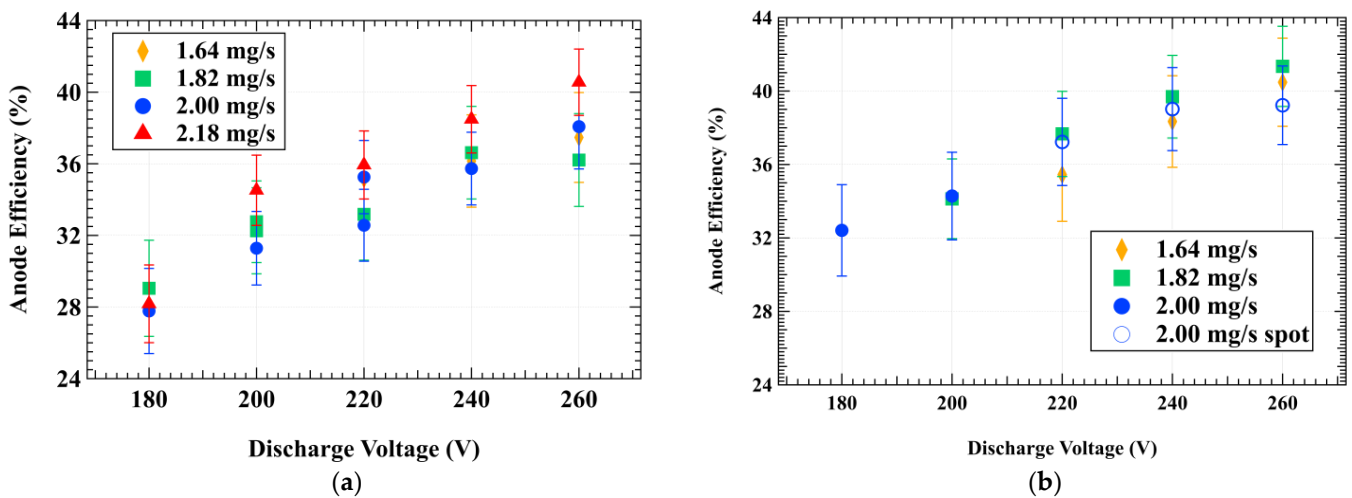


Figure 8. (a) Anode efficiency as a function of discharge voltage and anode mass flow rate for 5-s tests; (b) anode efficiency for the 15-s tests.

The effect of flow rate on efficiency is unclear from the data due to the measurement uncertainty. In the 15-s tests, it appears that the 1.64 mg/s flow rate resulted in higher efficiencies at discharge voltages above 200 V, while 2.00 mg/s was more efficient at the lower voltages. The 5-s data suggest that 2.18 mg/s flow resulted in the highest anode efficiency at all operating points except 180 V. No pattern is clearly discernable from these results, and the measurement uncertainties limit the significance of any identified trends with respect to flow rate.

3.5. Thrust to Power Ratio

Finally, the thrust-to-power ratio is shown in Figure 9. The thrust to power ratio is generally seen to decrease with increasing discharge voltage, with a peak at low voltages. As with anode efficiency, uncertainties limit the ability to draw conclusions about the relationship between anode flow and thrust to power ratio.

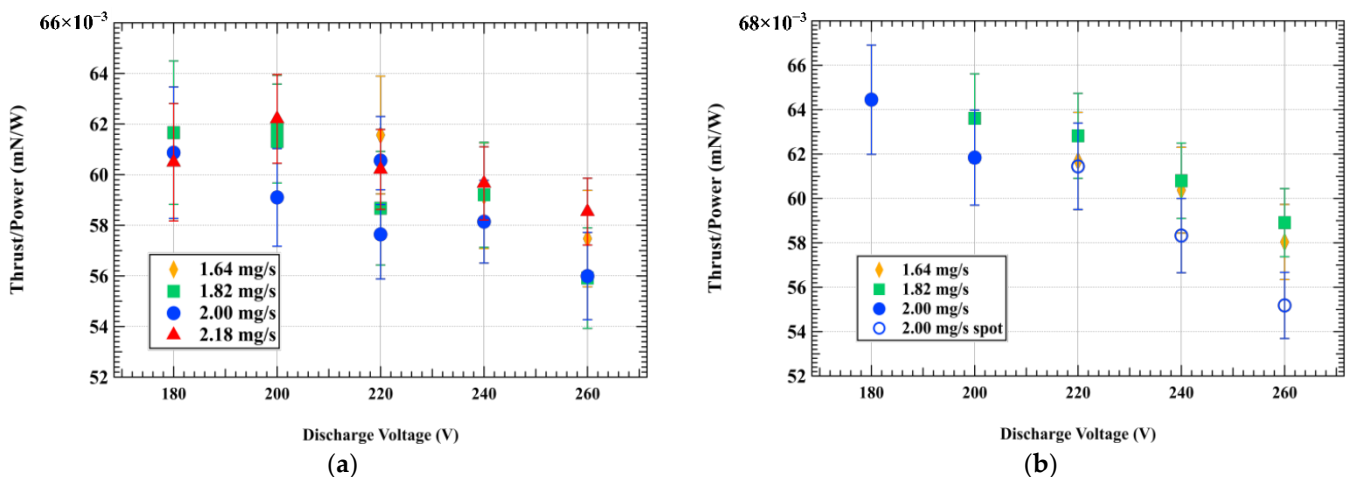


Figure 9. (a) Thrust-to-power ratio as a function of discharge voltage and anode mass flow rate for 5-s tests; (b) thrust-to-power ratio for the 15-s test.

3.6. Repeatability

While measurement uncertainty due to equipment error is quantified, a more significant challenge with transient testing is verifying that our methodology for comparing performance at different operating points is valid. The transient performance of the thruster

is sensitive to the thermal condition of the channel; therefore, we chose to compare performance at points where the thermal condition of the channel should be similar by looking at a fixed time after ignition. However, the heating rate and wall power losses in Hall thrusters also vary depending on the discharge voltage, since this affects electron temperature and consequently channel wall losses [9,12]. This effect could be a source of error since it could cause the outgassing to vary between tests.

Furthermore, the vacuum environment limits heat dissipation mechanisms, causing the channel to take a long time to return to ambient temperature after a test. In order to minimize the amount of propellant used for running the cathode, tests were run in sequences of four or five with five minutes between tests to allow the thruster to cool. For the 5-s tests, the pauses were adequate to allow the channel to cool between tests. However, the pauses were not adequate during the 15 s tests, and the cumulative heating from running at higher discharge powers eventually led to spot formation on the outer channel wall.

In an effort to characterize the impact channel temperature may have, we repeated tests at several operating points. Figure 10 shows four repeat thrust measurements at 200 V and 1.82 mg/s, which was the most-tested operating point.

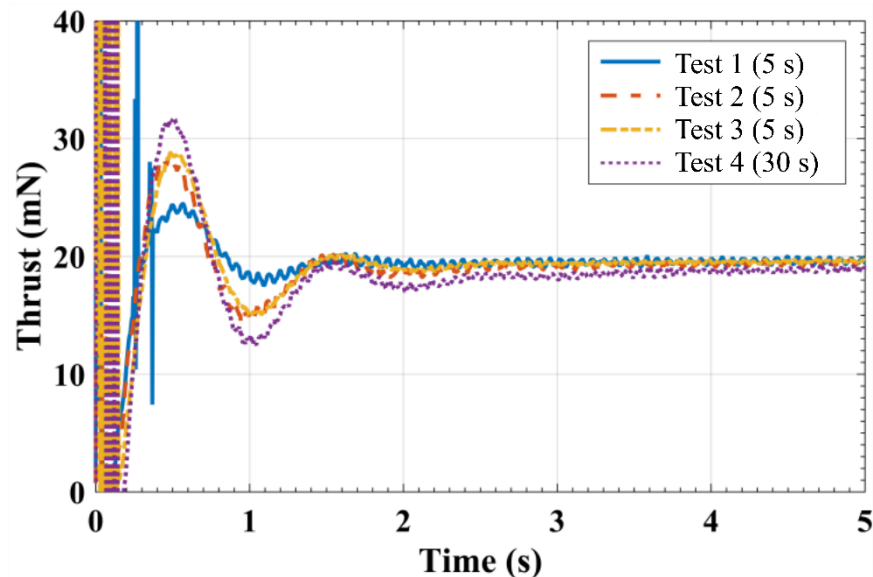


Figure 10. Repeat tests at 200 V and 1.82 mg/s anode mass flow.

The initial thermal condition of the channel was different for each of the repeat tests. For example, Test 2 was the last of a sequence of four 5-s tests, so the channel temperature should have been elevated above ambient conditions. Tests 1–3 show strong agreement and converge on a thrust of approximately 19.5 mN. Test 4 is noticeably lower than the first three tests. However, test 4 is a final 30-s run, and the thrust measurement eventually converges on a value within 0.2 mN of the first three tests. The behavior suggests that the outgassing contribution to thrust approaches a steady-state value that is stable over our short duration tests before spotting occurs. Similar behavior was seen with other repeat tests, providing some confidence that transient thruster performance can be compared across operating points.

3.7. Comparison with Other Low-Power Hall Thrusters

Table 3 provides a comparison of the performance parameters collected from the UAH-78AM to other Hall thrusters of similar power levels. The data are provided not to compare thruster performance, but to demonstrate that performance measurements of the UAH-78AM are comparable to experimental measurements of other 300–500 W Hall thrusters. Anomalous performance results would indicate that the unconventional design

features of the UAH-78AM were changing the performance in a manner that requires further testing and research to understand.

Table 3. Comparison of Thrusters in the UAH-78AM Power Class at Similar Discharge Voltages.

Thruster	VD (V)	Power (W)	Thrust (mN)	Anode I _{SP} (s)	Anode Efficiency (%)
MaSMi [17]	200–250	160–747	8.8–33	775–1321	21–29
SPT-50 [18]	199–282	210–389	12.9–18.9	1160–1524	35–41
BHT-200 [19]	200–275	200	11.5–12.5	-	35–42
ACE [20]		400	18	1300	
Aurora [21]	300	100–300	5.7–19	1080–1460	30–44
UAH-78AM	180–260	280–520	17–30	870–1450	27–42

4. Conclusions

A main goal of this work was to assess whether low-cost 3D printing with polymers or glazed ceramics can be used in the fabrication of Hall effect thrusters. In addition to reduced fabrication costs, 3D printing has the potential to open up the design space, as was done for liquid rocket engines. The ability to print complex geometries or internal passages could allow novel designs and configurations of Hall thrusters to be built. It is not known at this time what those designs may be, but the possibility is now there. The low cost and fast turnaround time of the UAH-78AM also shows a path toward a rapid design and test cycle for Hall thrusters. Changes to the design of a thruster to optimize the performance can be easily tested in the lab over multiple iterations at minimal cost of materials.

While the data collected cover only short duration testing, our results demonstrate that the UAH-78AM is capable of operating within normal jet-mode Hall discharge with performance comparable to other thrusters of a similar power and size. Therefore, by the most basic definition, the UAH-78AM is a fully functioning Hall Thruster, and 3D printing and other low-cost AM technologies can be used to build Hall thrusters.

However, for a Hall thruster to be useful, it must be capable of sustaining a continuous discharge for satellite propulsion. In the case of the UAH-78AM, current test durations are too short to collect plume data or steady-state thrust and temperature data using conventional methods. The only measurements that can be collected with the UAH-78AM are transient, since the steady state thermal operating condition for the thruster is beyond the temperature limits of the materials used for the channel. While transient data might be insightful for baselining the performance of a thruster, steady state data is ultimately needed for the development of flight hardware.

Another important consideration is that thruster design deficiencies of the UAH-78AM could be contributing to the short test durations. Channel wall heating and erosion in Hall effect thrusters are dependent on the magnetic field topology in the channel. Magnetically shielded field topologies have been found to reduce channel wall heating by reducing the contact between the plasma and the wall [22,23]. Our magnetic circuit design was based on an unshielded field topology for the purpose of simplicity; however, the unshielded design only increases thermal losses to the channel walls as compared to shielded designs.

Performance comparisons of the UAH-78AM with other thrusters of similar power levels and sizes were given in Table 3, two of which have been flown. The BHT-200 was flown onboard the TACSAT-2 (2006), FalconSat-5 (2010), and FalconSat-6 (2018) missions. It was slated to be flown on the Iodine Satellite (iSat) mission [24]. The SPT-50 was flown on the Canopus-V mission in 2012. This showed that the AM thruster, though it has some non-standard materials, was able to reach similar performance metrics as flight thrusters. The operational lifetime is a limitation, as mentioned, but this can be solved as AM technology advances. Small Hall thrusters have also been flown on small satellite missions including the ExoMG thruster (2020), and most notably SpaceX's krypton small Hall thruster used

in their Starlink constellation of satellites. However, no data on the Starlink thruster is currently available.

Future revisions of the thruster may explore applications for 3D printing in the design of the magnetic circuit. However, at this time, 3D printing of magnetic components is still an emerging technology with limited availability. Furthermore, many 3D printed magnet processes currently are focused on polymer-bonded magnets [25,26]. Bonded magnets generally have lower maximum energy product than metallic magnets [27], thus requiring larger magnets to produce the required magnetic field intensities. Other future work may include the use of high temperature 3D printable materials. Of special interest are the ceramic or metal impregnated PLA filaments that have become commercially available in the last few years. These filaments have 40–80% by mass of a filler material such as clay, zirconium silicate, copper, and iron. If the printed part is put into a debinding and sintering process, it may be possible to produce a fully ceramic or metal Hall thrust component while still using a desktop 3D printer.

Author Contributions: Conceptualization, E.P.H. and K.G.X.; methodology, E.P.H., W.H. and K.G.X.; software, E.P.H.; validation, E.P.H., W.H. and K.G.X.; formal analysis, E.P.H.; investigation, E.P.H.; resources, W.H. and K.G.X.; data curation, E.P.H.; writing—original draft preparation, E.P.H.; writing—review and editing, W.H. and K.G.X.; visualization, E.P.H.; supervision, W.H. and K.G.X.; project administration, K.G.X.; funding acquisition, W.H. and K.G.X. All authors have read and agreed to the published version of the manuscript.

Funding: E.P.H. was funded by the Alabama Space Grant Fellowship. The work at NASA GRC was supported by the LERCIP program.

Data Availability Statement: The supporting data will be provided upon request to the corresponding author.

Acknowledgments: The authors would like to thank the staff at the UAH Propulsion Research Center and NASA GRC for assisting in the work and making it possible.

Conflicts of Interest: The authors declare no conflict of interest.

References

1. Hall, S.J.; Florenz, R.E.; Gallimore, A.; Kamhawi, H.; Brown, D.L.; Polk, J.E.; Goebel, D.M.; Hofer, R.R. Implementation and Initial Validation of a 100-kW Class Nested-channel Hall Thruster. In Proceedings of the 50th AIAA/ASME/SAE/ASEE Joint Propulsion Conference, Cleveland, OH, USA, 28–30 July 2014; American Institute of Aeronautics and Astronautics: Reston, VA, USA, 2014.
2. Ibarzo, J.; Caro, I.; Marcos, J. Alternative manufacture technologies for the manufacture of HET larger ceramic chamber. In Proceedings of the 32nd International Electric Propulsion Conference, Wiesbaden, Germany, 11–15 September 2011; pp. 1–7.
3. Joshi, S.C.; Sheikh, A.A. 3D printing in aerospace and its long-term sustainability. *Virtual Phys. Prototyp.* **2015**, *10*, 175–185. [[CrossRef](#)]
4. Haas, J.M. Low-Perturbation Interrogation of the Internal and Near-Field Plasma Structure of a Hall Thruster Using a High-Speed Probe Positioning System. Ph.D. Dissertation, University of Michigan, Ann Arbor, MI, USA, 2001.
5. Dunaevsky, A.; Raitses, Y.; Fisch, N.J. Secondary electron emission from dielectric materials of a Hall thruster with segmented electrodes. *Phys. Plasmas* **2003**, *10*, 2574. [[CrossRef](#)]
6. Choueiri, E.Y. Fundamental Difference Between the Two Hall Thruster Variants. *Phys. Plasmas* **2001**, *8*, 5025–5034. [[CrossRef](#)]
7. Dunaevsky, A.; Raitses, Y.; Fisch, N.J. Yield of Secondary Electron Emission From Ceramic Materials of Hall Thruster With Segmented Electrodes. In Proceedings of the 28th International Electric Propulsion Conference, Foulouse, France, 17–21 March 2003; pp. 1–7.
8. Cazaux, J. A new model of dependence of secondary electron emission yield on primary electron energy for application to polymers. *J. Phys. D Appl. Phys.* **2005**, *38*, 2433–2441. [[CrossRef](#)]
9. Goebel, D.M.; Katz, I. *Fundamentals of Electric Propulsion: Ion and Hall Thrusters*; Jet Propulsion Laboratory: Pasadena, CA, USA, 2008.
10. Szabo, J.J.; Pote, B.; Tedrake, R.; Paintal, S.; Byrne, L.; Hrubby, V.J.; Kamhawi, H.; Smith, T. High Throughput 600 Watt Hall Effect Thruster for Space Exploration. In Proceedings of the 52nd AIAA/SAE/ASEE Joint Propulsion Conference, Salt Lake City, UT, USA, 25–27 July 2016; American Institute of Aeronautics and Astronautics: Reston, VA, USA, 2016.
11. Haag, T.W. Thrust stand for high-power electric propulsion devices. *Rev. Sci. Instrum.* **1991**, *62*, 1186–1191. [[CrossRef](#)]
12. Martinez, R.; Dao, H.; Walker, M.; Tech, G. Power Deposition into the Discharge Channel of a Hall Effect Thruster. *J. Propuls. Power* **2014**, *30*, 209–220. [[CrossRef](#)]

13. Hruby, V.; Monheiser, J.; Pote, B.; Rostler, P.; Kolencik, J.; Freeman, C. Development of low power Hall thrusters. In Proceedings of the 30th Plasmadynamic and Lasers Conference, Norfolk, VA, USA, 28 June–1 July 1999; American Institute of Aeronautics and Astronautics: Reston, VA, USA, 1999.
14. Santos, R.; Ahedo, E.; Raitses, Y.; Fisch, N.J. Transitional regime in the start-up process of conventional Hall thrusters. In Proceedings of the 32nd International Electric Propulsion Conference, Wiesbaden, Germany, 11–15 September 2011.
15. Polk, J.E.; Pancotti, A.; Haag, T.; King, S.; Walker, M.; Blakely, J.; Ziemer, J. Recommended practice for thrust measurement in electric propulsion testing. *J. Propuls. Power* **2017**, *33*, 539–555. [[CrossRef](#)] [[PubMed](#)]
16. Prichard, L.; Barwick, V. *Preparation of Calibration Curves A Guide to Best Practice Contact Point*; LGC Ltd.: Teddington, UK, 2003; pp. 1–27. [[CrossRef](#)]
17. Conversano, R.W.; Goebel, D.M.; Hofer, R.R.; Mikellides, I.G.; Katz, I.; Wirz, R.E. Magnetically Shielded Miniature Hall Thruster: Design Improvement and Performance Analysis. In Proceedings of the 34th International Electric Propulsion Conference, Kobe, Japan, 4–10 July 2015; pp. 1–12.
18. Manzella, D.; Oleson, S.; Sankovic, J.; Haag, T.; Semenkin, A.; Kim, V. Evaluation of low power hall thruster propulsion. In Proceedings of the 32nd Joint Propulsion Conference and Exhibit, Lake Buena Vista, FL, USA, 1–3 July 1996. [[CrossRef](#)]
19. Hruby, V.; Monheiser, J.; Pote, B.; Freeman, C.; Connolly, W. Low Power, Hall Thruster Propulsion System. In Proceedings of the 26th International Electric Propulsion Conference, Kitakyushu, Japan, 17–21 October 1999; Volume IEPC-99-09.
20. Apollo Fusion. Available online: <https://apollofusion.com/index.html> (accessed on 8 August 2021).
21. Sommerville, J. Performance of the Aurora Low-Power Hall-Effect Thruster. In Proceedings of the 36th International Electric Propulsion Conference, Vienna, Austria, 15–20 September 2019; pp. 1–7.
22. Mikellides, I.; Katz, I.; Hofer, R.; Goebel, D. Design of a Laboratory Hall Thruster with Magnetically Shielded Channel Walls, Phase II: Experiments. In Proceedings of the 48th AIAA/ASME/SAE/ASEE Joint Propulsion Conference and Exhibit, Atlanta, Georgia, 30 July–1 August 2012; pp. 1–26. [[CrossRef](#)]
23. Goebel, D.M.; Hofer, R.R.; Mikellides, I.G.; Katz, I.; Polk, J.E.; Dotson, B.N. Conducting wall hall thrusters. *IEEE Trans. Plasma Sci.* **2015**, *43*, 118–126. [[CrossRef](#)]
24. Dankanich, J.W.; Polzin, K.A.; Calvert, D.; Kamhawi, H. The iodine satellite (iSAT) Hall thruster demonstration mission concept and development. In Proceedings of the 50th AIAA Joint Propulsion Conference, Cleveland, OH, USA, 28–30 July 2014; pp. 1–13.
25. Huber, C.; Abert, C.; Bruckner, F.; Groenefeld, M.; Muthsam, O.; Schuschnigg, S.; Sirak, K.; Thanhoffer, R.; Teliban, I.; Windl, R.; et al. 3D Print of Polymer Bonded Rare-Earth Magnets, and 3D Magnetic Field Scanning With an End-User 3D Printer. *Appl. Phys. Lett.* **2016**, *109*, 162401. [[CrossRef](#)]
26. Li, L.; Tirado, A.; Nlebedim, I.C.; Rios, O.; Post, B.; Kunc, V.; Lowden, R.R.; Lara-Curzio, E.; Fredette, R.; Ormerod, J.; et al. Big Area Additive Manufacturing of High Performance Bonded NdFeB Magnets. *Sci. Rep.* **2016**, *6*, 36212. [[CrossRef](#)] [[PubMed](#)]
27. Ma, B.M.; Herchenroeder, J.W.; Smith, B.; Suda, M.; Brown, D.; Chen, Z. Recent development in bonded NdFeB magnets. *J. Magn. Mater.* **2002**, *239*, 418–423. [[CrossRef](#)]